J. Synchrotron Rad. (1998). **5**, 606–608

Front-end *XY*-slits assembly for the SPring-8 undulator beamlines

M. Oura,* Y. Sakurai and H. Kitamura

JAERI-RIKEN SPring-8 Project Team, The Institute of Physical and Chemical Research (RIKEN), Kamigori-cho, Ako-gun, Hyogo 678-12, Japan.
E-mail: oura@sp8sun.spring8.or.jp

(*Received 4 August 1997; accepted 28 October 1997*)

A front-end *XY*-slits assembly has been designed for the SPring-8 undulator beamlines. This assembly can handle the high heat flux from the undulator, its grazing-incidence L-shaped configuration employing an enhanced heat-transfer technology.

Keywords: undulator beamlines; front ends; high-heat-load components; XY-slits assemblies.

1. Introduction

The front-end *XY*-slits assembly (FE-SLIT) is one of the high-heat-load components in the SPring-8 undulator beamlines (Sakurai *et al.*, 1995; Kitamura, 1996). The main objective of the FE-SLIT is to reduce the heat load on the Be windows and first optical element by cutting off the off-axis part of the undulator beam. It consists of a set of L-shaped slits equipped with precision horizontal and vertical linear actuators and associated bellows for lateral movement, as shown in Fig. 1.

The L-shaped slit will be impinged by a very intensive undulator beam with 451 kW mrad^{-2} peak heat flux in the worst case. To handle such a high heat flux, the L-shaped slit has been designed to be of a grazing-incidence configuration so as to stretch out the heat load on the slit-blade. In order to reduce the heat load on the slit-blade further, the assembly is installed downstream of the pre-slit assembly (Takahashi *et al.*, 1998), whose circular-aperture exit is 4 mm in diameter, and the graphite filters assembly (Sakurai *et al.*, 1995). Even if the aperture size is limited by the pre-slit, the FE-SLIT should handle almost 5 kW of radiated power when the undulator gap is set to be minimum.

In this article, we describe the design features of the FE-SLIT and its thermomechanical properties. The installation of the assembly and its utilities are also described.

2. Design features of the FE-SLIT

The design of the shape of the grazing-incidence slit-blade is based on the APS-L5 slit (Shu *et al.*, 1995), with suitable modifications for direct cooling. The grazing-incidence angle is fixed at 1.57° on the vertical blade surface. This angle will decrease the peak power from 540 to 14.8 W mm^{-2} on the slit-blade. The slit-blade is made of a single Glidcop block and is formed as part of the inner wall of the vacuum vessel. Both ends of the Glidcop block are explosively bonded to stainless-steel UHV joints. Fig. 2 shows a conceptional view of the FE-SLIT. The upstream *XY*-slit consists of left-vertical and lower-horizontal blades. The downstream *XY*-slit consists of right-vertical and upper-horizontal blades. Each slit block has two cooling channels and is water-cooled; the convective heat transfer coefficient is enhanced by the use of copper mesh brazed into the cooling channels (Kuzay *et al.*, 1991). Each slit block is mounted on an *X* translation (transverse to the beam and in a horizontal axis) stage and a *Z* translation (transverse to the beam and in a vertical axis) stage to allow the vessels to be positioned with respect to each other such that a rectangular aperture size can be adjusted. The FE-SLIT can be manipulated into a variety of aperture shapes with sizes from 10 × 8 down to 0 mm (H) × 0 mm (V) by controlling the *XZ* actuators. As we can see in Fig. 2, the aperture size can be set to enable most photons of fundamental radiation to pass through the FE-SLIT but most waste photons to be shut off. The aperture size of the FE-SLIT, however, should be determined to secure safety in utilizing downstream components such as Be windows and/or a first optical component (Oura *et al.*, 1998).

Each actuator, which is motor-controlled, has a datum switch and two limit switches. These limit switches are set to avoid over-run resulting in accidental irradiation onto parts of the downstream beamline components. The resolutions of linear motion of the *X*-stage and the *Z*-stage are 1 and 0.25 μm pulse^{-1}, respectively.

3. Thermomechanical analysis

As was mentioned in §1, the FE-SLIT should handle almost 5 kW of radiated power in the most severe condition, even if the pre-slit restricts the aperture to a circular diameter of 4 mm. In order to understand the thermomechanical properties of the *XY*-slit regarding maximum surface temperature and thermal stress, finite-element analyses were performed using *ANSYS* for some cases of full irradiation onto the vertical blade and partial irradiation, in which the aperture of the FE-SLIT was set to 2 × 1, 1 × 0.5 and 0 mm (H) × 0 mm (V). The dependence of the surface temperature and the thermal stress on the aperture size were studied.

In the *ANSYS* finite-element analyses, a model of the *XY*-slit was made for an L-shaped blade, whose length was 77% of the final design in the beam direction, having two cooling channels. The modelled *XY*-slit was assumed to be located at 30 m from the light source and 2 m downstream of the pre-slit assembly. The spatial distribution of the absorbed power was approximated by

$$F(h, v) = (2^{1/2}P_T/\pi^{3/2}\sigma_v W_h)\exp(-v^2/2\sigma_v^2)(1 - h^2/W_h^2)^{1/2}\delta(h, v),$$

where h and v are, respectively, the horizontal and vertical distances measured from the centre of the beam axis, P_T is the total power, σ_v is the standard deviation of the spatial distribu-

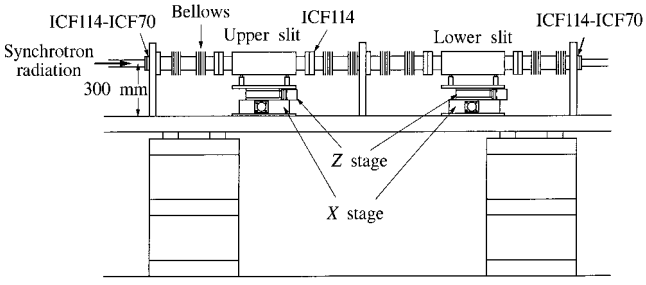

Figure 1
Schematic view of the FE-SLIT.

Table 1
Properties of the material and quantities used in the analyses.

Young's modulus, E (GPa)	130
Poisson ratio, ν	0.326
Thermal conductivity, k (W m^{-1} K^{-1})	365
Thermal expansion coefficient, α (10^{-6} K^{-1})	16.6
Total power, P_T (kW)	10.7
σ_v at XY-slit (mm)	1.193
W_h at XY-slit (mm)	4.929

tion of the radiated power in the vertical direction, W_h is the half width of the spatial distribution of the radiated power in the horizontal direction, and $\delta(h,v)$ is the δ function, which becomes unity when the coordinate (h,v) resides in the projection of the pre-slit on the XY-slit. Table 1 shows the material properties and the quantities used in the analyses. We assumed a convective heat-transfer coefficient of 15 000 W m^{-2} K^{-1} in conservative calculation. The temperature of the cooling water was assumed to be 303 K.

3.1. *Maximum surface temperature and thermal stress*

3.1.1. *Full irradiation onto the vertical blade.* In the *ANSYS* calculation, the location of the beam centre was assumed to be at the centre of the vertical blade. This situation is, however, the special case in which the X-stage overruns due to an accident or it is actuated intentionally. The calculated maximum temperatures of the vertical blade and the surface of the cooling channel are about 510 and 373 K, respectively. The corresponding maximum equivalent stress, *i.e.* Mise's equivalent stress, is calculated to be about 254 MPa.

In the case of irradiation onto the horizontal blade, the footprint of the beam extends much more than in the case of vertical-blade irradiation, so that the resulting maximum temperature for the same cooling condition is less severe.

3.1.2. *Partial irradiation.* The results from the *ANSYS* calculation are summarized in Table 2. In the case of zero aperture size, all the photon beam is cut by the upstream XY-slit and the downstream XY-slit with the ratio 3:1, respectively. Although this situation is the most severe case possible in normal operation of the beamline, the corresponding maximum equivalent stress is less than the yield strength of Glidcop (SCM Metal Products, 1994).

When the aperture of the FE-SLIT is set to allow the most photons of fundamental radiation to pass through, the resulting maximum equivalent stress may be much less than the yield strength. In such a situation, however, we should notice that there is some thermal distortion along the L-shaped edge of the slit-blade leading to a small change in the aperture size of the FE-SLIT. Estimation for such a problem strongly depends on the condition of restraint. A rigorous analysis is in progress.

Table 2
Maximum temperature and maximum equivalent stress under partial irradiation.

T_b^{max} is the maximum temperature on the blade surface, T_c^{max} is the maximum temperature on the surface of the cooling channel, σ_e^{max} is the maximum equivalent stress.

Aperture size (mm^2)	T_b^{max} (K)	T_c^{max} (K)	σ_e^{max} (MPa)
0 (0 × 0)	470	344	248
0.5 (1 × 0.5)	431	331	197
2 (2 × 1)	379	317	121

4. Installation of the assembly and its utilities

The centre of the FE-SLIT is located at 28.9 m from the undulator and the total length of the assembly is 1.935 m. A photograph of the FE-SLIT is shown in Fig. 3. This is installed inside the shielding wall and is located downstream of the pre-slit assembly and the graphite filters assembly so as to reduce waste photons on the slit-blade. A separate water-cooling system is mounted on the common base just beneath the assembly. This

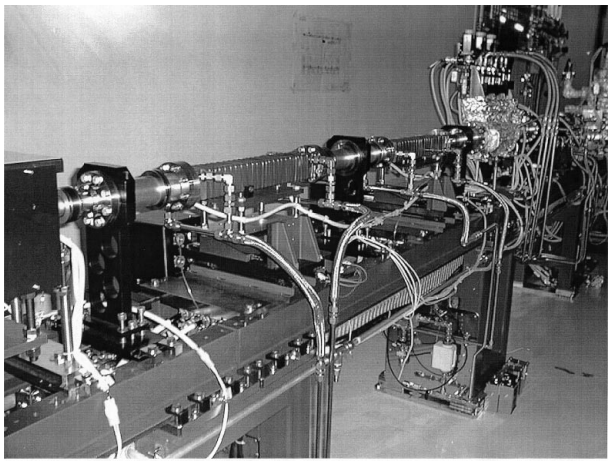

Figure 3
Photograph of the FE-SLIT installed on the common base of the SPring-8 front end. View from the downstream.

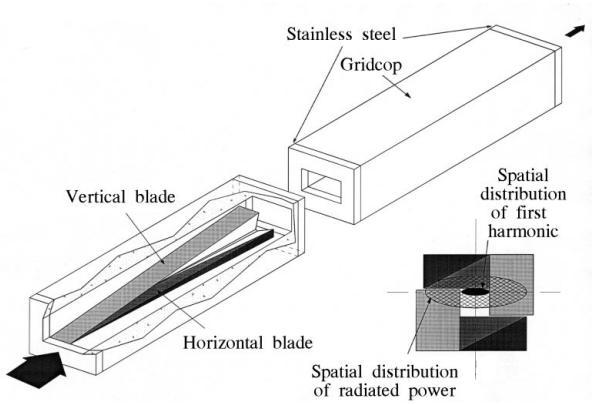

Figure 2
Conceptual drawing of the FE-SLIT.

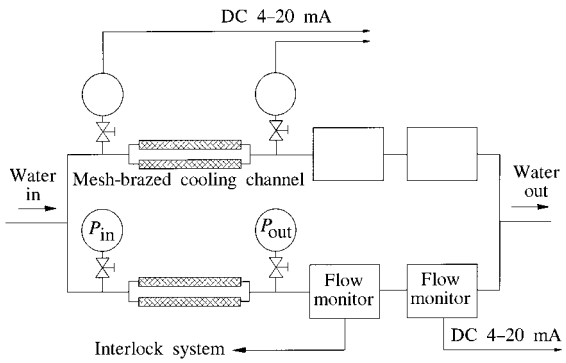

Figure 4
Schematic drawing of the water-cooling system.

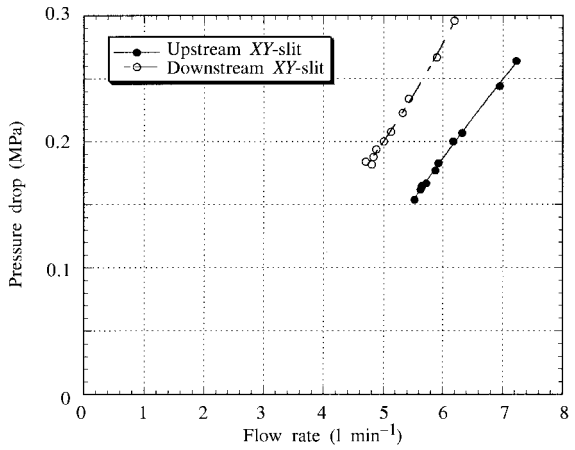

Figure 5
Relationship between the pressure drop and the flow rate of the cooling water.

consists of two cooling manifolds and flexible stainless-steel hosing for connection to the slit bodies *via* Swagelok connectors. Each manifold has two pressure gauges and two different types of flow monitor. Fig. 4 shows a schematic drawing of the water-cooling system. The pressure gauges and one of the flow monitors give outputs of 4–20 mA DC. By using those outputs, we can monitor both water pressures (P_{in} and P_{out}) and the flow rate outside the shield wall. We can also obtain information about the pressure drop ($P_{in} - P_{out}$) due to the mesh brazed inside the cooling channel. After the installation of the first *XY*-slits assembly into the front end of the pilot undulator beamline (BL47XU), we measured the pressure drop of the cooling water as a function of the flow rate. Fig. 5 shows the relationship between the pressure drop and the flow rate. The flow rate in abscissa is for the gross water flowing in two cooling channels. The pressure drop is proportional to the square of the flow rate and the friction factor, which depends on the Reynolds number. Since there are so many influencing factors, it is not easy to discuss quantitatively the curves in Fig. 5. We can suppose, however, a heat-transfer coefficient by making a comparison with the experimental data obtained by the APS group (Kuzay, 1996). For the cooling channel we expect that as much as a four- to fivefold increase in the heat-transfer coefficient relative to a plain channel is possible.

References

Kitamura, H. (1996). *HOSHAKOU*, **9**, 403–412. (In Japanese.)
Kuzay, T. M. (1996). Private communication.
Kuzay, T. M., Collins, J. T., Khounsary, A. M. & Morales, G. (1991). *ASME/JSME Thermal Engineering Proceedings*, Vol. 5, pp. 451–459. ASME (Book No. 10309E-1991).
Oura, M., Sakae, H., Sakurai, Y. & Kitamura, H. (1998). *J. Synchrotron Rad.* **5**, 609–611.
Sakurai, Y., Oura, M., Sakae, H., Usui, T., Kimura, H., Oikawa, Y., Kitamura, H., Konishi, T., Shiwaku, H., Nakamura, A., Amamoto, H. & Harami, T. (1995). *Rev. Sci. Instrum.* **66**, 1771–1773.
SCM Metal Products (1994). *Catalogue of Glidcop*, SCM Metal Products, Inc., Research Triangle Park, North Carolina, USA.
Shu, D., Brite, C., Nian, T., Yun, W., Haeffner, D. R., Alp, E. E., Ryding, D., Collins, J., Li, Y. & Kuzay, T. M. (1995). *Rev. Sci. Instrum.* **66**, 1789–1791.
Takahashi, S., Sakurai, Y. & Kitamura, H. (1998). *J. Synchrotron Rad.* **5**, 581–583.